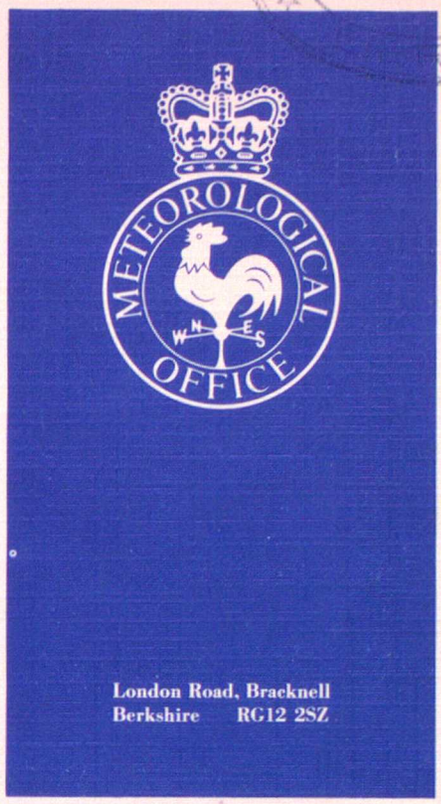


LONDON, METEOROLOGICAL OFFICE
Met.O.15 Internal Report 70

Observations of bright band.

05911086 FH5B

An unpublished document
Not to be quoted in
print.

METEOROLOGICAL OFFICE
London Road, Bracknell, Berks.

# MET.O.15 INTERNAL REPORT

No 70

## OBSERVATIONS OF BRIGHT BAND

by

G P Cox and S A Clough

Cloud Physics Branch (Met.O.15)
September 1986

KW

Observations of Bright Band G.P. Cox and S.A. Clough

## 1. Introduction

The extensive spatial coverage of precipitation information provided by radar is used in many fields including hazardous weather detection, forecasting of precipitation areas and hydrological measurements. Accurate quantitative measurements, which may be required in such applications, rely upon prediction of the precipitation rate from observed reflectivity. A simple Z-R relationship such as:-

$Z=200R^{1.6}$ (Marshall and Palmer, 1948)

is generally used and may give quite reliable estimates of precipitation rate when the radar observes rain. For example Harrold et al (1974) observed errors of typically 37% in estimated hourly rainfall amounts. Errors are likely to be much greater however if the radar beam intersects either snow or melting snow. The Z-R relationship shown above becomes inappropriate because of the lower refractive index of ice and more complex particle distribution. As a result of the low fallspeed of ice particles, relatively high concentrations of hydrometeors are found above and within the melting zone. Consequently, aggregation of particles and the increasing refractive index of melting elements within the melting layer may lead to reflectivities of up to 10 times those seen in either the ice region above or rain area below. On a PPI scan this phenomena appears as a

ring of high reflectivity around the radar commonly known as the bright band. One way of still obtaining quantitative precipitation measurements after having identified the bright band is to correct the observed reflectivity using an assumed vertical reflectivity profile (Smith, 1983). The accuracy of the corrective procedure will be a strong function of the model bright band profile used and thus a more detailed knowledge of bright band climatology (Smith, 1983) and a thorough understanding of relevant microphysical processes are required to enable improvements to be made in current corrections.

The interaction of microphysical processes within the melting layer is complex and many important facets of the transformation between solid and liquid hydrometeors are not well documented. Particle aggregation and breakup and the mechanics of particle melting and collapse are not well understood. The relative importance of these processes varies with hydrometeor type and size such that the bright band is often seen to change greatly over distances of only a few kilometres. Computational models predicting the form of the bright band therefore have little general predictive skill since their results are strongly dependent upon the numerous assumptions required to describe the ice hydrometeors and their melting behaviour.

One potential way of increasing understanding of these processes within the bright band is through the use of dual polarisation radar. In addition to the effective reflectivity, the dual polarisation radar at Chilbolton currently measures differential reflectivity (ZDR), the ratio of horizontal to vertical reflectivities, which gives some measure of the

density, asymmetry and alignment of hydrometeors (Bader et al 1986). ZDR returns in rainfall depend solely upon rain dropsize distribution and are well understood (Seliga and Bringi, 1976) but as with reflectivity this is not the case in the melting layer.

In this note we discuss aircraft and dual polarisation radar observations of the melting layer. The Meteorological Office's C130 aircraft flew to the West of the Chilbolton radar and simultaneous dual polarisation and in-situ microphysical measurements were made in light stratiform precipitation. Observations above the melting layer from the same flight were presented by Bader et al (1986). The main aim of this study is to report and interpret changes of the radar profile in the bright band as precipitation rate and type vary.

In 1983 the Maypol experiments provided some important observations of the melting layer from linearly and circularly polarised radars. Moninger et al (1984) noted that a single peak in ZDR was generally observed below the maximum in reflectivity and that the vertical separation between the peaks increased with precipitation rate. In certain cases a second peak in ZDR above the peak in Z was also seen. From changes in CDR and $\rho$ (the cross correlation) Moninger and co-workers deduce that changes in the variance of the canting angle of melting hydrometeors are responsible for the observed trends in ZDR, though their interpretation in terms of the actual physical processes responsible is unclear. Atlas (1984) argues that the parameter $\rho$ has been misinterpreted by Moninger et al and that high values of ZDR at the base of the melting layer are due to the few remaining large melting flakes which are oriented and wet. The observations reported

do not allow a firm conclusion. It seems likely that the latter approach is correct since microphysical studies (Ono, 1969; Cho et al, 1981; Magono and Nakamura., 1965) have shown that both single crystals and asymmetric aggregates are likely to fall in a stable configuration with their largest axis horizontal. We present here images of melting particles which also support the interpretation of Atlas. In this study we identify three different bright band archetypes. Using the Atlas model we are able to interpret the observed structure of the bright bands in terms of hydrometeor type and melting behaviour.

In section 2 we describe the experiment and observations. In section 3 we present our results and attempt to account for variations in terms of relevant physical processes. Finally in section 4 conclusions are drawn.

## 2. Instrumentation and Experiment

The data presented in the following sections were obtained during an experiment carried out in conjunction with members of the Rutherford and Appleton Laboratory on the 15th of May 1984. The experimental data consists primarily of dual polarisation radar measurements from the Laboratory's Chilbolton Observatory in southern England and also simultaneous in-situ microphysical observations from the C130 aircraft (Readings, 1985). The dual polarisation radar at Chilbolton has a 25 metre antenna with 0.25° beam width and operating frequency of 3076.5MHz, the data samples being range gated to provide 300m radial average values of Z and ZDR (Hall et al, 1984).

2-D Knollenberg image probe observations, Johnson Williams liquid water contents and temperature data are available from the aircraft. The cloud (2D-C) and precipitation probes (2D-P) were both used (Knollenberg, 1970). The former samples particles passing through a 0.8mm window across the flight track with nominal resolution of 25μm whilst the latter has 6.4mm window with 200μm resolution. The 2D data and subsequent analysis provide 2 dimensional images, spectra and bulk parameters such as rainfall rate, which are derived through the application of Cunningham's, (1978) formulae for a chosen precipitation type. Due to the sensitivity of bulk parameters to assumptions of habit and density they should best be regarded as semi-quantitative.

During the flight the aircraft made 10 level runs along a radial track to the West of Chilbolton. The stratiform precipitation observed was uniformly light (< 1mm/hr) and lasted throughout the period of the experiment. Wind information is available from the nearby Larkhill radiosonde ascent, and also the aircraft's own observations. Both sources indicate that the winds above the melting layer were predominantly East South Easterly with approximately unidirectional light shear (~1m/s/km), consistent with radar observations of precipitation trails which moved in a westerly direction during the day. Further flight and meteorological details are available in Bader et al (1986). The observations described in this work were obtained from 4 of the 10 passes, 2 of which took place above the melting layer. Passes above the melting layer are particularly useful since images of 'dry hydrometeors' are more easily classified and spectra and bulk parameters are more reliable.

## 3. Results

### I. Radar and Aircraft Observations of the Bright Band

In this section we present results from the 2 aircraft runs above the melting layer together with appropriate radar data. The first run is at an average temperature of -2°C and the second run is at -0.5°C. In order to directly compare hydrometeors observed above the melting layer with radar observations of the melting layer itself, range corrections are applied to take account of the hydrometeor trajectory in the relevant layer. Additionally a further correction must be made to account for the movement of the system as a whole in the short period between radar and microphysical observations. Numerous radar 'hits' pinpoint the position of the aircraft to within 300m so that when the appropriate corrections are applied to the two runs, radar observations of the bright band and microphysical observations from above it are closely comparable. The inevitable errors caused by evolution of the precipitation system and falling hydrometeors have been minimised by ensuring that the aircraft is close to the melting layer and that the RHI scan is made during the run. The RHI radar scans for the 2 runs are presented in figure 1. Notice the higher reflectivity trails above 2 km in the first example which outline the positions of fallstreaks. As the fallstreaks intersect the melting layer at a height of 1.4 km their higher concentrations of crystals and generally greater precipitation rates intensify the radar bright band in Z. The structure of the ice phase precipitation in the second example is less clear though there is a significant bright band at a height of 1.4 km. In figure 2 the equivalent rainfall rates for both runs (with range corrected

to 1.4 km height) are shown. The precipitation rates given by 2D data for both examples are roughly 50% lower than those predicted by the Sekhon-Srivastava (1970) Z-R relationship for snow, a result which seems acceptable considering the semi-quantitative nature of bulk parameters and their sensitivity to universal assumptions concerning particle type and density. In example 1, two precipitation maxima can be seen, one at 35 km and a second at 46 km corresponding to the 2 fallstreaks which are clearly defined in the radar reflectivity at upper levels. The rainfall rate in example 2 exhibits an extended maximum suggesting 2 merging fallstreaks though with no further information firm conclusions cannot be drawn. Particle distributions for both examples show that larger, faster falling elements have a downshear bias, probably resulting from a shear sorting process (Gunn and Marshall, 1954). The largest particles in both examples are small aggregates of several crystals only.

Theoretical studies of the bright band (eg Dissanayake et al, 1983) predict a strong positive correlation between precipitation rate and peak reflectivity. We compared the precipitation rates obtained from the 2D system with the peak bright band reflectivity of appropriate profiles averaged over 3 consecutive range gates (900m), to test this hypothesis. This averaging process reduces some of the high local variability of the bright band providing a better indication of general trends. The correlation coefficient between $Z_{max}$ and precipitation rate was found to be 0.83: highly significant for a sample of 30 points. Additionally we find that increasing precipitation rates reduce the height of peak reflectivity (correlation coefficient; -0.43). The least squares regression lines are shown in figure 3.

In comparing the precipitation rate with bright band profile we observe 3 types of bright band and define each archetype as follows:-

Type 1 Peak values of Z and ZDR occur within 100m height of each other.

- Observed in light precipitation (<0.3mm/hr)

Type 2 Double peak in ZDR, one peak above maximum Z and one peak below maximum Z.

Observed in precipitation ~ 0.3 mm/hr.

Type 3 Peak in ZDR lower than peak Z.

Observed in precipitation heavier than 0.3 mm/hr.

See Figure 4 for illustrations. Microphysical details of these archetypes are examined in the following section. The distribution of the 3 archetypes over the two aircraft runs is illustrated in figure 5. Note that the third type of bright band occurs only in heavier precipitation and is therefore not seen in example 2. The 0.3 mm/hr threshold observed in this study is unlikely to be the same from one system to another but as becomes evident below, should be indicative of the behaviour to be expected in stratiform precipitation. Observational Studies e.g. Moninger et al (1984), indicate that this type of bright band is most common when the precipitation is heavier.

## II. Microphysical Observations of Melting behaviour

Figure 6 shows images of hydrometeors observed within the melting region during the third and fourth passes. Bulk parameters obtained by the 2D system are unreliable in the melting region so the precipitation rates of each sample have been inferred using the regression relationship between peak reflectivity and precipitation (figure 3). We have chosen samples having similar precipitation rates so that the differences between each are probably due to the melting process rather than any initial diversity of precipitation type and size. In the first sample at +0.7°C the rounded form of single crystals and aggregates suggests that smaller elements are already water coated. No elements larger than 200μm are entirely water, though by +1.1°C droplets of 600μm can be seen and remaining ice elements are virtually indistinguishable . Finally at +3.1°C the only surviving solid elements are large smooth edged aggregates.

The observation that large hydrometeors penetrate comparatively further into the melting region than smaller ice elements is not surprising. Firstly, the greater thermal capacity of large elements extends their melting time (eg. see Donovan, 1982) and secondly their higher terminal velocity should carry them further into the warmer air before melting is complete. Note also that melting and mass loading effects will allow parcels with heavier precipitation, and thus more large particles, to penetrate further into the melting layer. Descending through the melting layer the most reflective elements are increasingly large hydrometeors which become electromagnetically wet in turn. Also meltwater

may form into an oblate spheroid (Fukuta et al, 1983). This simplification of the melting process may allow us to interpret features of the bright band more readily. It is important however to recognize that the profile is a result of the evolution of a distribution of melting particles rather than identical elements.

## III. Microphysical Interpretation of Bright Band profiles

### Type 1

This archetype was observed in light precipitation (<0.35 mm/hr) and Z and ZDR peaks occur at the same height.

The most reflective elements in type 1 bright bands are apparently those which also give high values of ZDR when partly melted, which suggests that the precipitation consists principally of single crystals. 2D data from the second example of type 1 bright band (figure 7) is consistent with this suggestion indicating that fewer than 70 elements per cubic metre exceed 2.5 mm.

As single crystals begin to melt they become water coated and their refractive index is rapidly increased. This would lead to increases in reflectivity of approximately 7dB for a solid ice sphere (Kerker, et al 1951) though in practice as melting proceeds the axial ratios and thus drag coefficients of crystals are also reduced. The consequent increase in fallspeed reduces the concentration of reflecting elements and, for single crystals, the increasing reflectivity is unlikely to achieve the 7dB

predicted. This weak bright band characteristic of single crystals can be seen in figure 7. Peak ZDR values are theoretically greatest when planar crystals of high density (Dissanayake et al, 1983) are present though the $D^6$ dependence of the reflectivity factors $Z_H$ and $Z_V$ implies that observed ZDR values tend to be dominated by the largest elements present. Below peak reflectivity the decreasing axial ratio and consequently increasing fallspeed of melting elements reduces Z and ZDR simultaneously.

Type 2

This archetype was observed in light precipitation (~ 0.3 mm/hr). There are peaks in ZDR above and below maximum reflectivity (eg figure 4b). The various height regions depicted in figure 4 can be considered in terms of physical processes as follows:

A-B Z increases from 20 to 24 dB and ZDR decreases due to crystal growth and especially aggregation. The minimum value of ZDR seems to be a good indicator of the top of the melting layer.

B-C Z increases to 29dB due to the increase of refractive index on melting and continued aggregation.

ZDR increases rapidly to 1.0dB probably because aligned single crystals very rapidly become 'wet'. An oblate element with a refractive index approaching that of water may produce high ZDR (Fig 8).

C-D Z continues to increase as larger hydrometeors become electromagnetically wet, though single crystals begin to collapse and the reduction in axial ratio gives the observed fall in ZDR to 0.8 dB. The increasing reflectivity of aggregates with axial ratios nearer to 1 will also dilute ZDR values.

D-E Z decreases as the ice structure of hydrometeors begins to collapse. Small crystals fully melt to droplets likely to have zero ZDR (see figures 8, 9). As aggregates melt Fukuta et al (1983) observe the formation of a central oblate water core, which seems likely to be the cause of the increase of ZDR at this height. The peak value of ZDR (1.1) corresponds theoretically to an aligned and oblate water element having an axial ratio of about 0.9 (figure 8).

E-F Both Z and ZDR decrease as all elements finally collapse to droplets. The value of ZDR below the melting layer is dependent upon the dropsize distribution as ZDR is purely a function of droplet size. (figure 9).

We believe that this description is the most likely explanation of the type 2 profile. Unlike Moninger et al (1984) we do not see the need to invoke changes in the stability of particle motion to describe such a profile, though our explanation does require the formation of a stable oblate ice/water core in the final stage of aggregate melting. This is certainly suggested by the images in Figure 6.

Type 3 This archetype was observed in heavier precipitation (0.35 mm/hr→0.5 mm/hr) and has a single peak in ZDR below the peak reflectivity (eg figure 4c).

Archetype 3 can be explained using similar arguments to archetype 2. The upper peak in ZDR is not visible in the type 3 bright band, probably because the relative contribution to the reflectivity by small aligned hydrometeors is reduced in heavier precipitation, ie larger aggregate particles mask expected high ZDR returns. In heavier precipitation (~ 0.3 mm/hr) aggregates become more common. Yokoyama and Tanaka (1984) calculate that reflectivity may increase by up to 15 dB as they melt due to the vast change in the refractive index of the low density ice air structure as it becomes water coated. As precipitation rate and the number of aggregate particles increases the difference between maximum reflectivity and the reflectivity of the ice precipitation may thus exceed 7dB. Greater aggregation within the melting layer will also enhance the reflectivity (Stewart et al, 1984) though the increase of terminal velocity will tend to reduce it. The bright band occurs at a slightly lower level in heavier precipitation because larger elements take longer to melt and also because a high flux of melting particles is capable of lowering the zero degree isotherm (Atlas et al, 1969). Moninger et al (1984) note that the separation between Z and ZDR peaks increases with precipitation rate. While this sample was too limited to see such behaviour it seems likely that oblate water cores are formed late in the melting process and only become evident when the bulky reflective hydrometeors which dominate Z and ZDR collapse. As peak ZDR values appear to be confined to the base of the

melting region, in heavier precipitation a wider spectrum of melting particles which will deepen the bright band will also tend to separate Z and ZDR peaks.

## 4. Conclusions

The main aim of this study was to report and interpret variations of the dual polarisation radar profiles (Z, ZDR) in the bright band as precipitation rate and character change. In order to do this dual polarisation radar measurements and simultaneous aircraft observations were made and observations were compared on kilometre scales. At this time we are limited specifically to bright band interpretation in light stratiform precipitation (<0.5mm/hr) having adequate data from one flight only.

In this study we observe three characteristic dual polarisation radar profiles in the melting layer. In very light precipitation (<0.25 mm/hr) the peaks in Z and ZDR are simultaneous because many of the particles associated with maximum reflectivity exhibit preferred alignment (eg planar crystals, Cho et al, 1981). This we call archetype 1. In very light precipitation (~0.1 mm/hr) the increase in reflectivity on melting is often seen to be less than 7dB suggesting that melting particles are relatively dense single crystals and that aggregation is not active. The maximum value of ZDR apparently depends upon the masking particles (Bader et al, 1986) and type of single crystal present.

As the precipitation rate and width of particle spectrum increases the level of maximum reflectivity is lowered. The reduction in height is presumably due to real depression of the melting layer and the presence of increasingly large elements which become electromagnetically wet at lower levels. A second peak in ZDR is observed below the level of maximum reflectivity because of the collapse of melting hydrometeors to an oblate ice/water structure late in the melting process. This is the second archetype.

In heavier precipitation (> 0.35 mm/hr) the upper peak in ZDR is lost because the relative contribution to ZDR of single crystals is reduced by more reflective quasi-spherical aggregates. The third archetype thus has a single ZDR peak below the level of maximum reflectivity. Studies of bright band (eg Illingworth, 1986) have indicated that this is the most common profile in heavier precipitation suggesting that our description of bright band may be more widely applicable to stratiform conditions in general. It is clear, however, from the complexity of the behaviour seen here that a numerical model corresponding to the spectral description developed here would be of limited value because of the large number of descriptive parameters required compared to relatively little observational data on any one case. However a statistical description based upon a number of cases may be more generally applicable.

REFERENCES


Atlas, D., Tatehira, R., Srivastava, R.C. and Carbone, R.C. 1969 Precipitation induced mesoscale wind perturbations in the melting layer. QJRMS, pp 544.

Atlas, D. 1984 Highlights of the Symposium on the multiple-parameter radar measurements of precipitation: Personal reflections. Radio Science 19 number 1. 238-243.

Bader, M.J., Clough, S.A. and Cox, G.P. 1986 Aircraft and dual polarisation observations of hydrometeors in light stratiform precipitation. Submitted to Quarterly Journal of the Royal Met Soc.

Cho, H.R., Iribarne, J.V. and Richards, W.G. 1981 On the orientation of ice crystals in a cumulonimbus cloud. J.Atmos. Sci, 38, 1111-1115.

Cunningham, R.M. 1978 Analysis of particle spectral data from optical array (PMS) 1D and 2D sensors. 4th Symp Met Obs and Inst Apr 10-14; Boston, Mass; Amer. Met. Soc.

Dissanayake, A.W., Chandra, M. and Watson, P.A. 1983 Prediction of differential reflectivity due to various types of ice particles and ice water mixtures. London Inst. Elec. Engineers Internal Conf. Antenna Propagation Conf. Publ. 219, 12-15 Apr, Norwich.

Donovan, G.J. 1982 Melting of natural snowflakes, suspended in a vertical wind tunnel, M.S. Thesis, University of Utah.

Fukuta, N., Savage, R.C., Donovan, G.J. and Lill, C.M. 1983 The microphysics of snow crystal and snowflake melting. AFGL-TR 83-0066, AD A129030.

Gunn, K.L.S. and Marshall, J.S. 1954 The effect of wind shear on falling precipitation. J. Met, 12, 339-349.

Hall, M.P.M., Goddard, J.W.F. and Cherry, S.M. 1984 Identification of Hydrometeors and other targets by dual-polarisation radar. Radio Sci, 19; 132-141.

Harrold, T.W., English, E.J. and Nicholass, C.A. 1974 The accuracy of radar-derived rainfall measurements in hilly terrain. Q.J.R.M.S, 100. pp 331-350.

Illingworth, A. 1986 Personal communication.

Kerker, M., Langleben, P. and Gunn, K.L.S. 1951 Scattering of microwaves by a melting spherical ice particle. J Meteor. Amer. Met. Soc. 8, p. 424.

Knollenberg, R.G. 1970 The optical array: An alternative to scattering or extinction for airborne particle size determination. J Appl Meteor 9, 86-103.

Magono, C. and Nakamura 1965 Aerodynamic studies of falling snowflakes. J Meteor Soc Japan 43, 139-147.

Marshall, J.S. and Palmer, W M K 1948 The distribution of raindrops with size. J. Meteor. 5, pp 165-166.

Moninger, W.R., Bringi, V.N., Jordan, J.R., Seliga, T.A. and Aydin, K. 1984 Melting layer observations during Maypol. 22nd Conf. Radar Met. 364-370.

Ono, A. 1969 The shape and riming properties of ice crystals in natural clouds. J. Atm. Sci., 26, 138-147.

Readings, C.J. 1985 The use of aircraft to study the atmosphere: the Hercules of the Meteorological Research Flight. Met. Mag. 114, 66-78.

Sekhon, R.S. and Srivastava, R.C. 1970 Snow size spectra and radar reflectivity. J. Atm. Sci., 27, 299-307

Seliga, T.A. and Bringi, V.N. 1976 Potential use of radar differential reflectivity measurements at orthogonal polarisations for measuring precipitation. J. Appl. Meteor., 15, 69-76.

Smith, C.J. 1983 The reduction of errors caused by bright band in quantitative rainfall measurements using radar. Research Report 38 Met Office Radar Research Lab.

Stewart, R.E., Marwitz, J.D., Pace, J.C. and Carbone, R.E. 1984 Characteristics through the melting layer of stratiform clouds. J. Atmos. Sci, 41, 3227-3237.

Yokoyama, T. and Tanaka, M. 1984 Microphysical processes of melting snowflakes detected by two-wavelength radar. J Meteor. Soc. Japan. 62, 4, 650-678.

CAPTIONS

1a. RHI Reflectivity scan for the aircraft run at a temperature of -2°C.

1b. RHI Differential Reflectivity scan for the aircraft run at a temperature of -2°C.

1c. RHI Reflectivity scan for the aircraft run at a temperature of -0.5°C.

1d. RHI Differential Reflectivity scan for the aircraft run at a temperature of -0.5°C.

2. Precipitation Rates along both runs diagnosed from the 2D Knollenberg probe data.

3a. Precipitation Rate vs peak reflectivity; least squares regression line.

3b. Precipitation Rate vs height of bright band; least squares reqression line.

4. Illustrations of bright band archetypes.

5. Distribution of the archetypes along the two runs studied.

6. Images of melting hydrometeors; precipitation rate ≈0.3 mm/hr.

7. Illustration of a weak, type 1 bright band and images of ice crystals from above it.

8. The ratio of backscatter cross sections $\delta m/\delta v$ for an oblate spheroidal scatterer as a function of its axis ratio. The dashed portion of the line for a liquid is at ratios where drops are unstable; however, it can be used for water-coated ice. (From the Gans theory.)

9. The ratio of the major axis length to minor axis length (b/x).

RUN HEIGHT 1.9KM : TEMPERATURE -2C

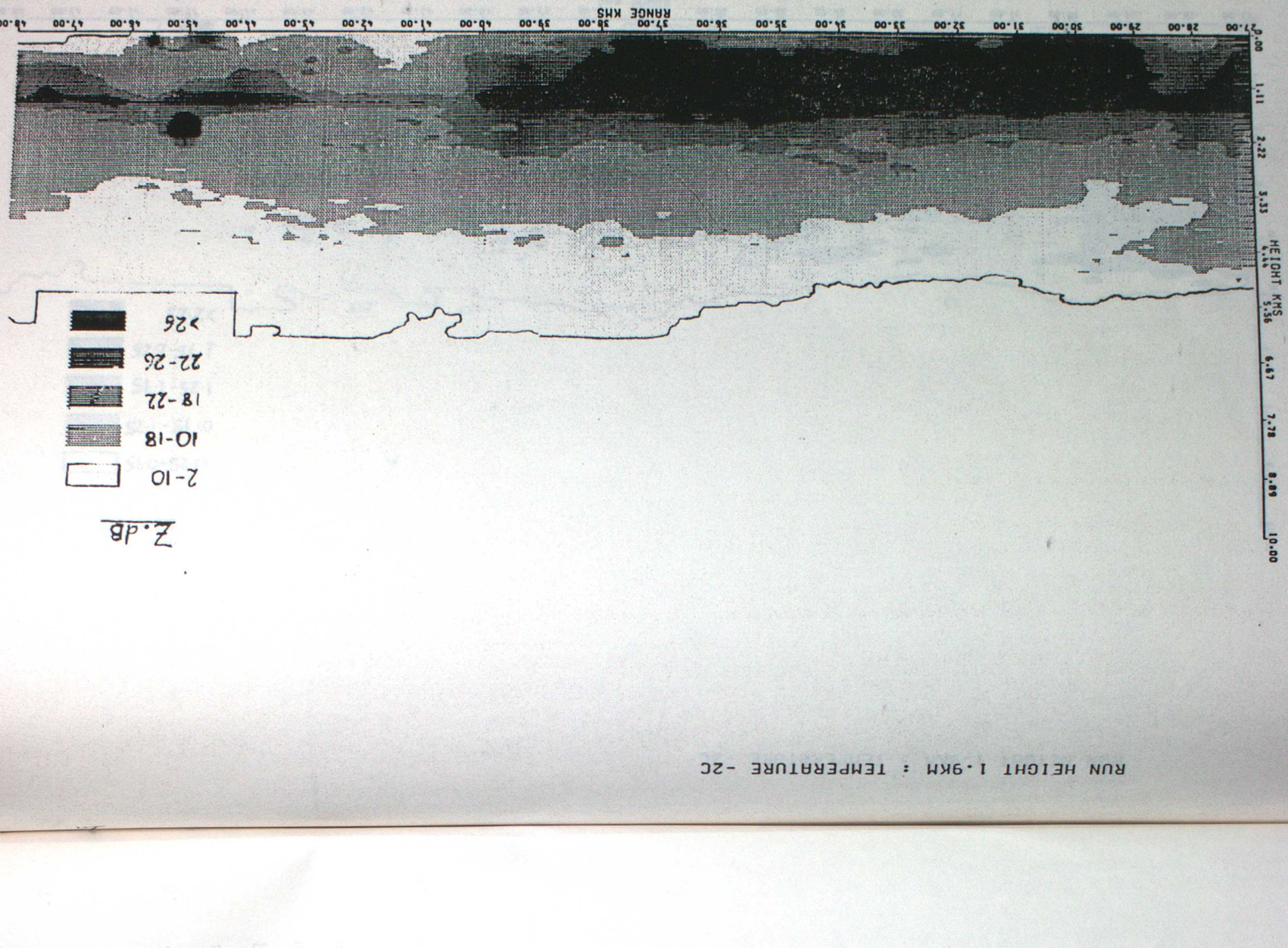

RUN HEIGHT 1.9KM : TEMPERATURE -2C

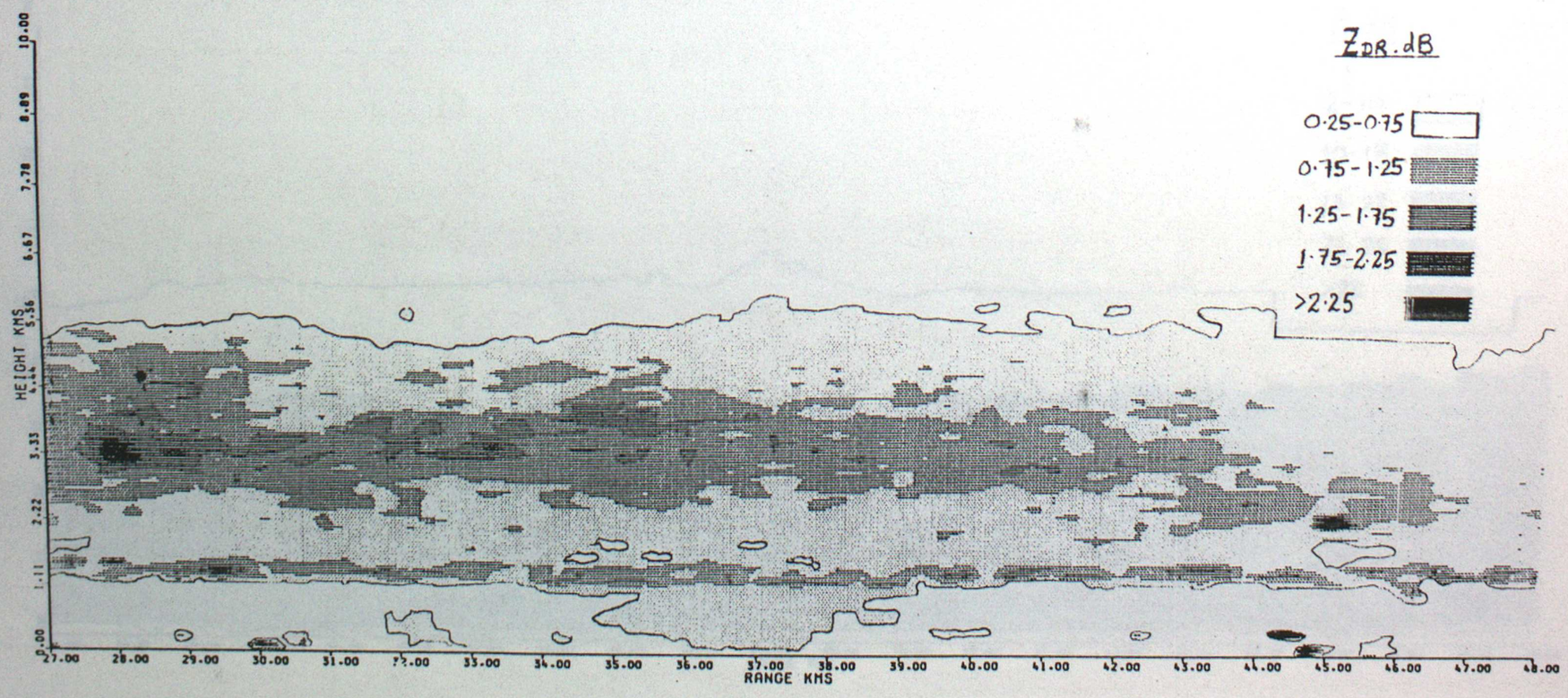

RUN HEIGHT 1.5KM : TEMPERATURE -0.5C

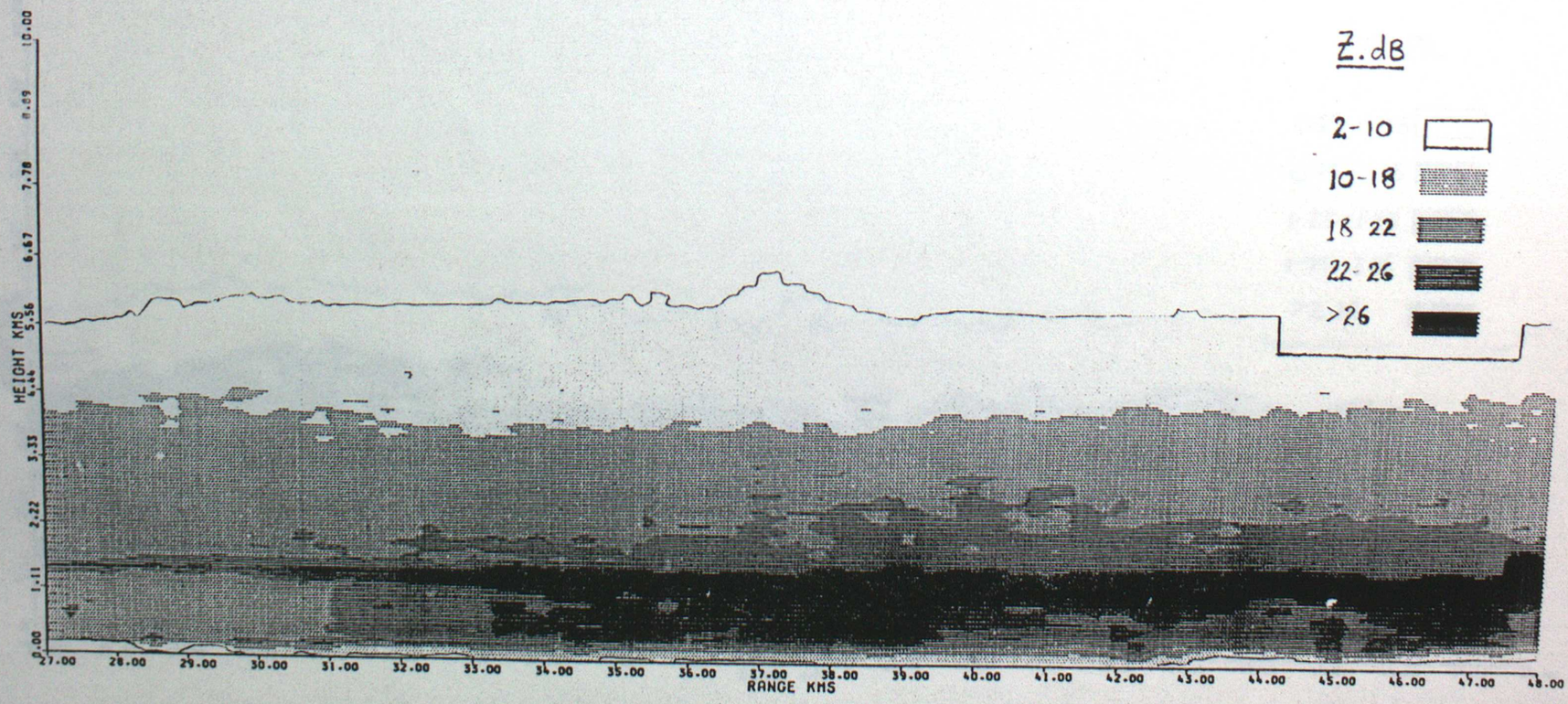

RUN HEIGHT 1.5KM : TEMPERATURE -0.5C

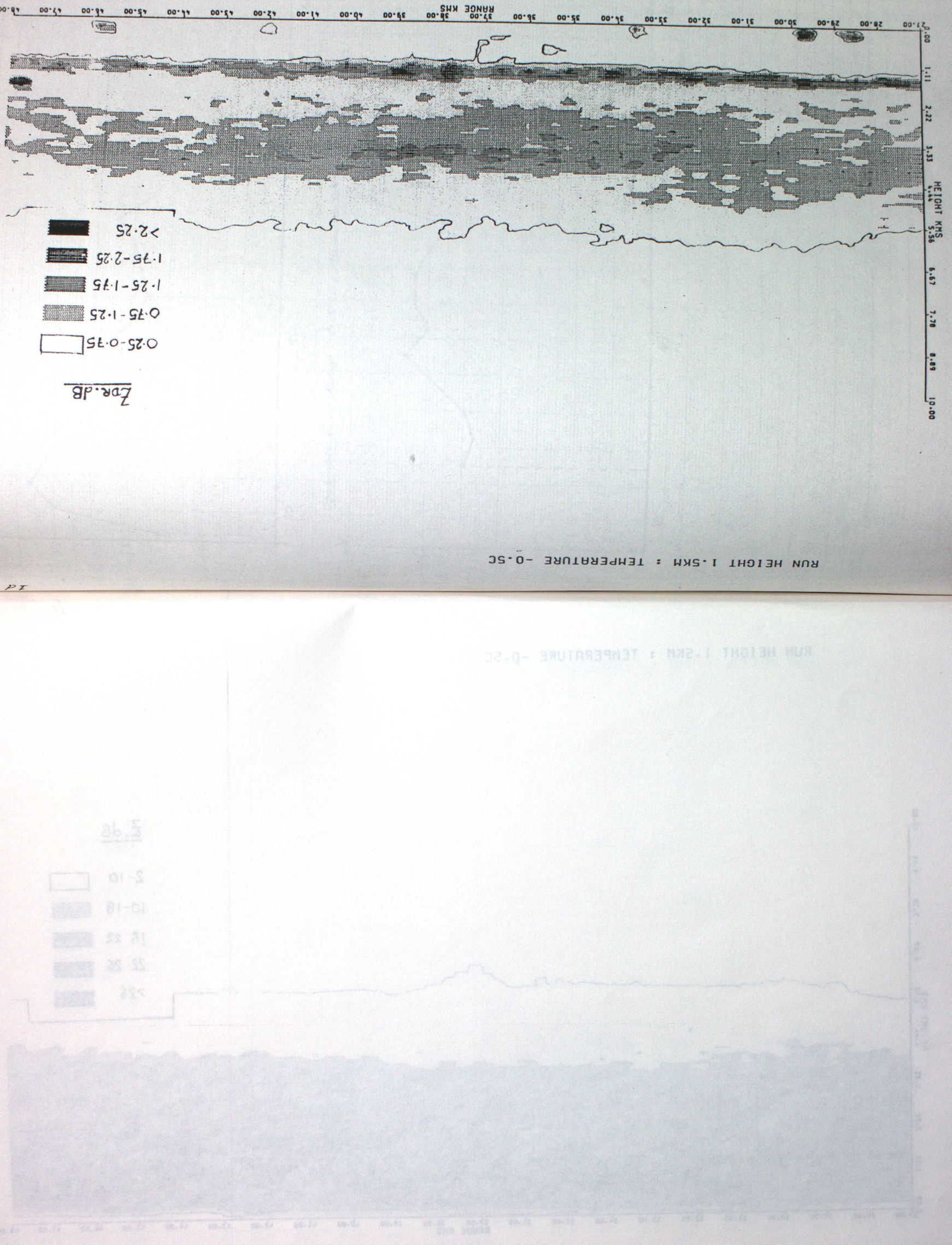

Figure 2.

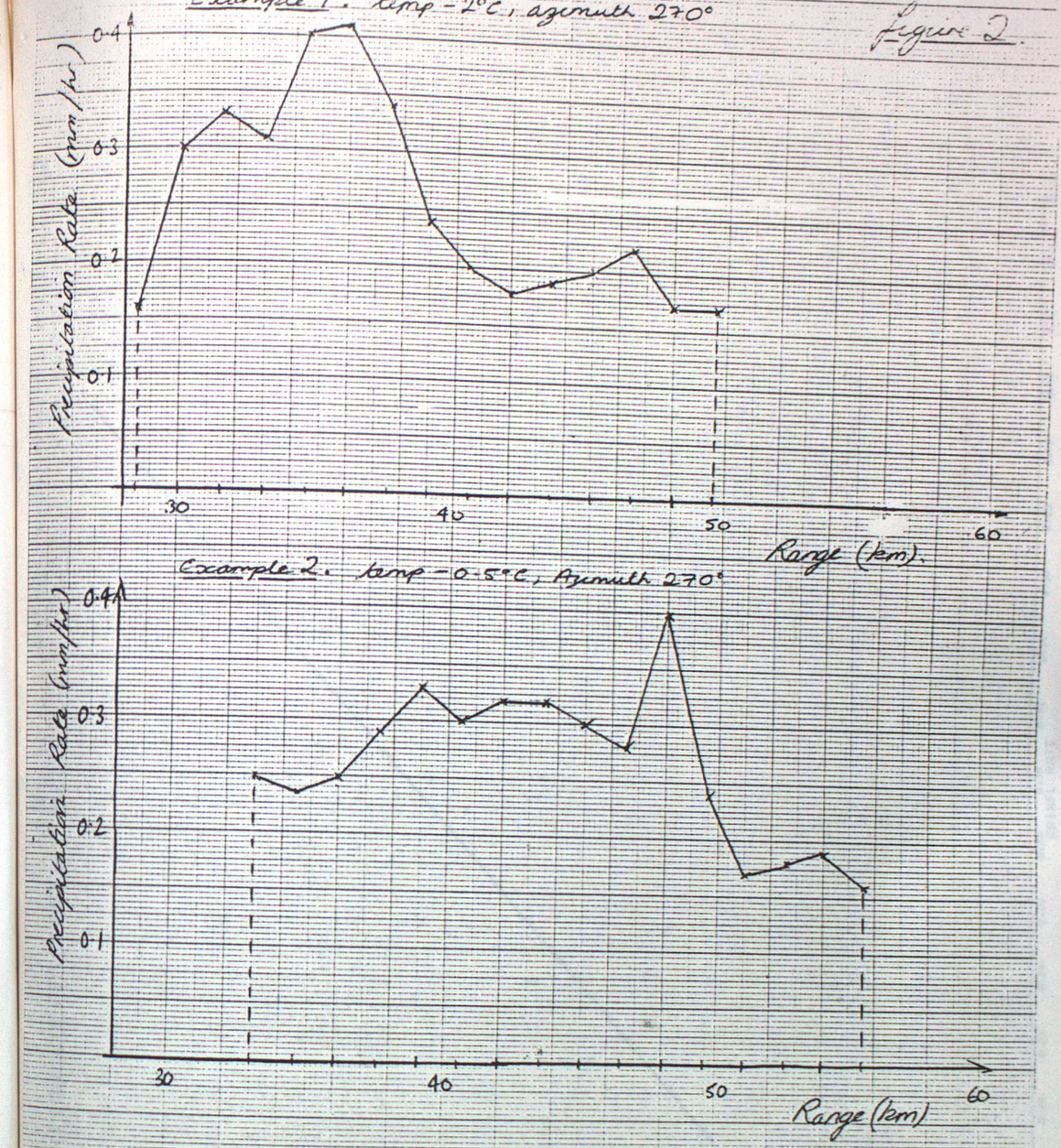
Example 1. temp -2°C, azimuth 270°
Precipitation Rate (mm/hr)
0·4
0·3
0·2
0·1
30
40
50
60
Range (km).
Example 2. temp -0·5°C, Azimuth 270°
Rate (mm/hr)
Precipitation
0·4
0·3
0·2
0·1
30
40
50
60
Range (km)

3a

LEAST SQUARES REGRESSION LINE : Z MAX=44.044*RAINFL RATE+17.562
CORRELATION COEFFICIENT= 0.827

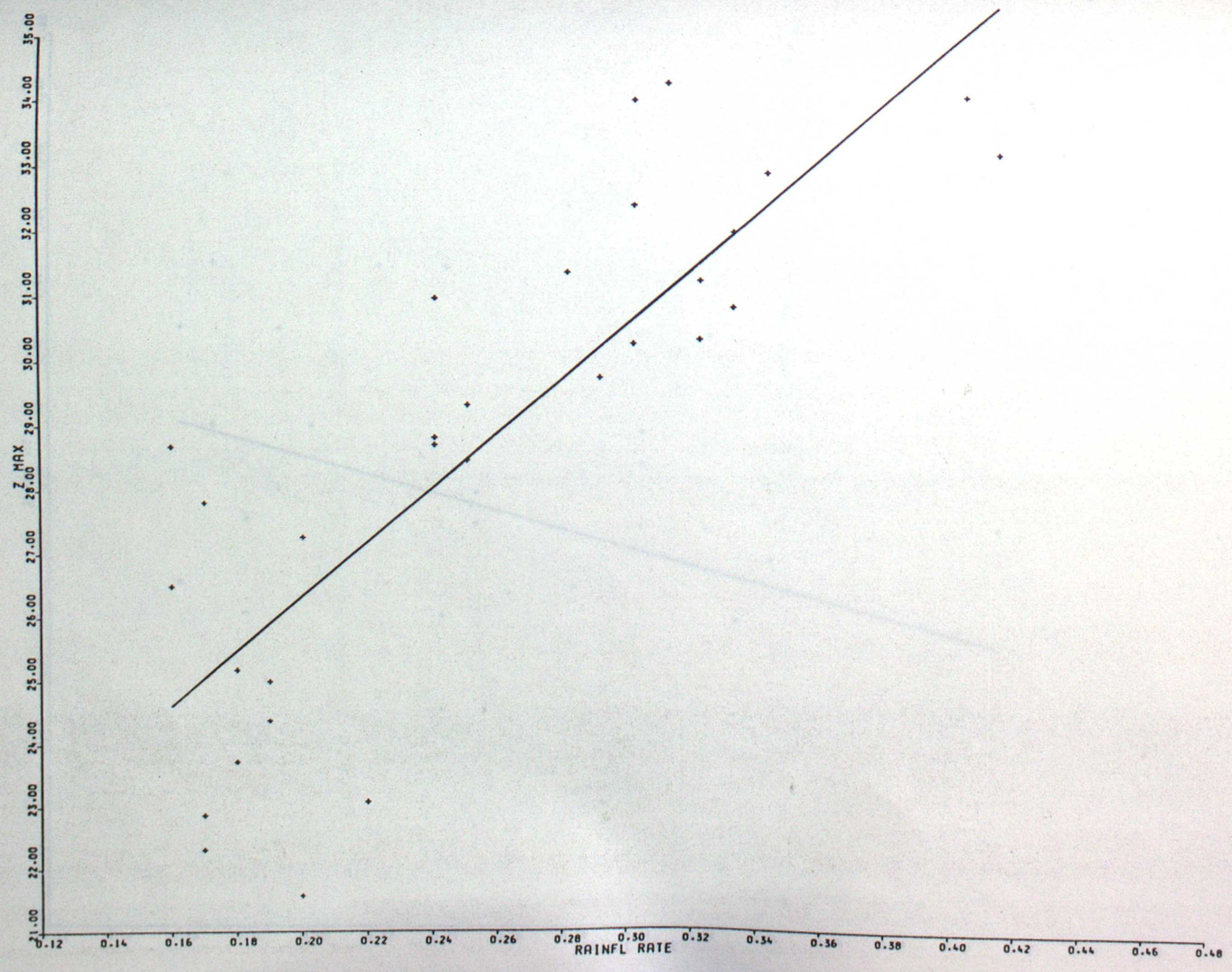

LEAST SQUARES REGRESSION LINE : Z MAX HT=-0.273*RAINFL RATE+1.544
CORRELATION COEFFICIENT= -0.429

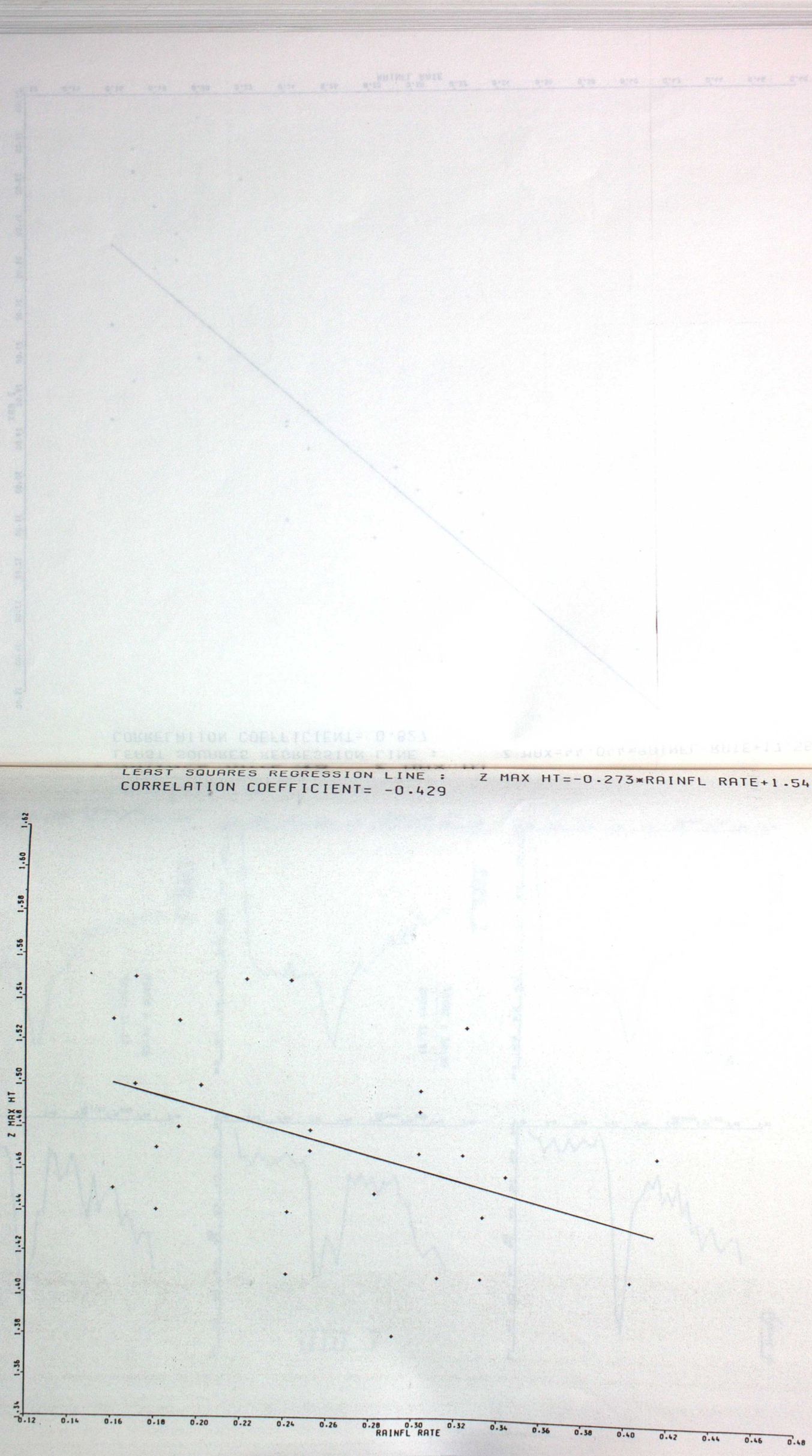

figure 4

TYPE 1

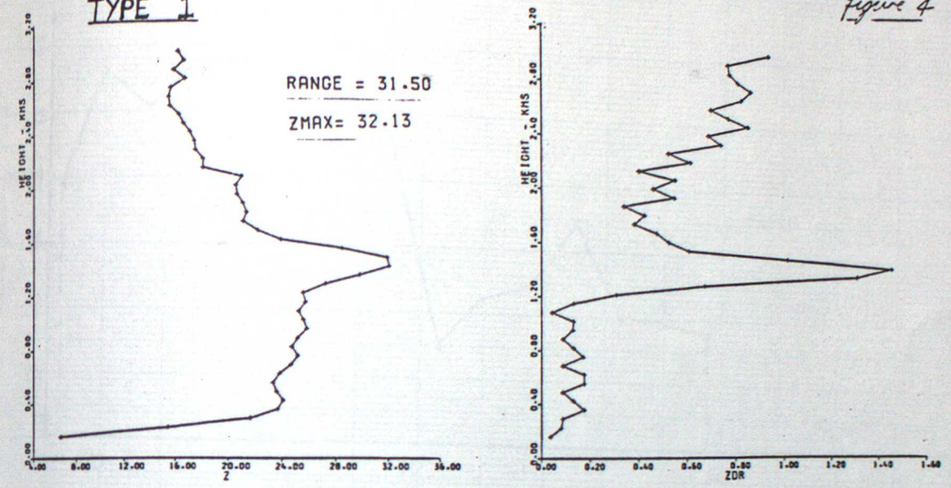


TYPE 2

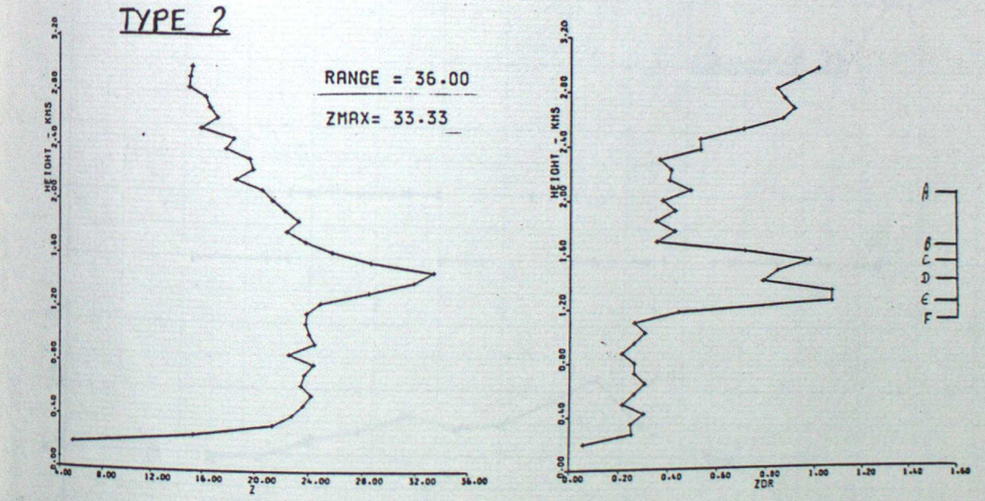


TYPE 3

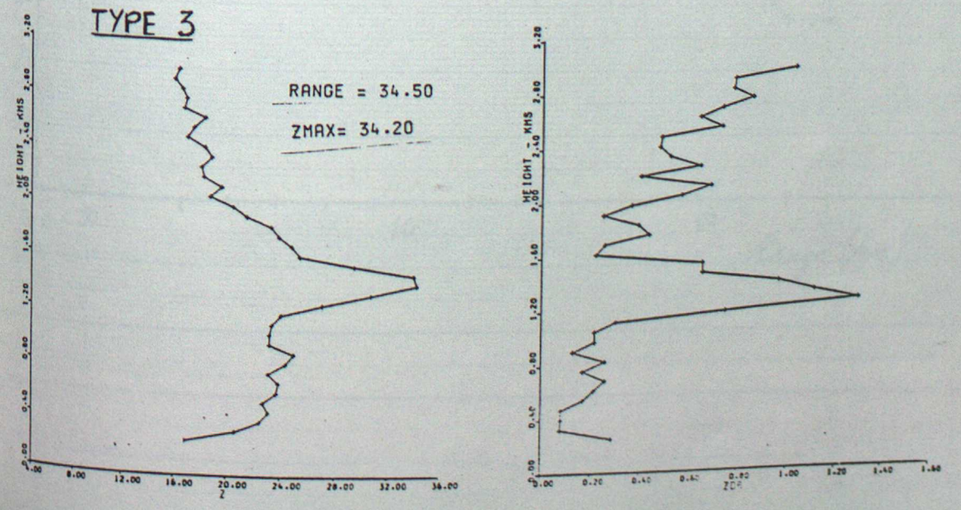

FIGURE 5.

Example 1.

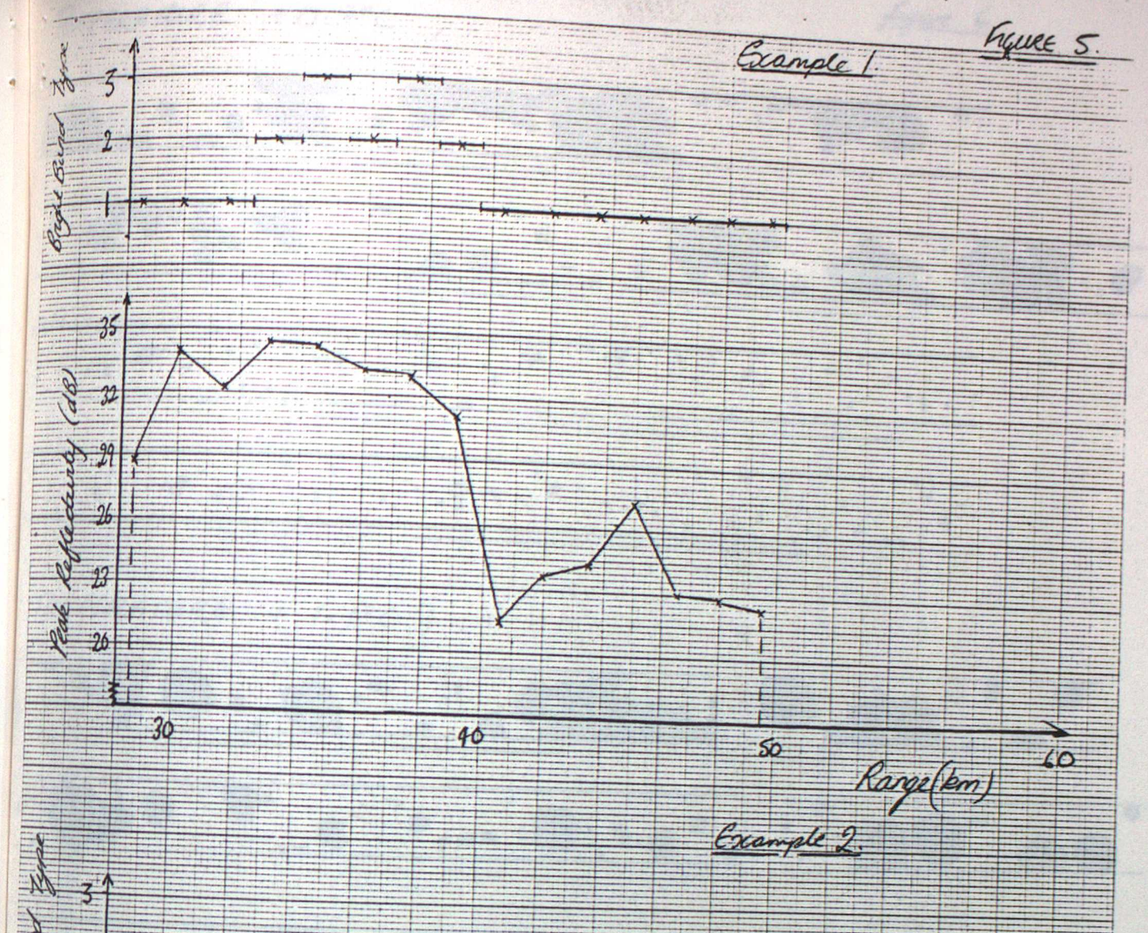


Example 2.

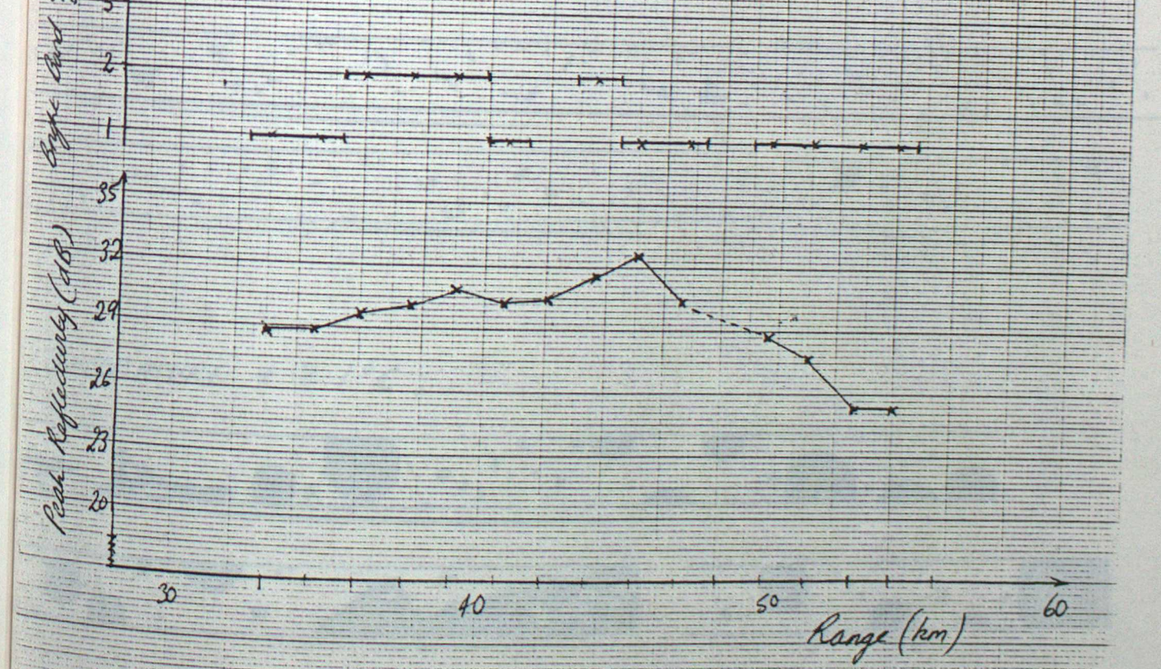

Figure 6

TEMPERATURE +0.7°C ;

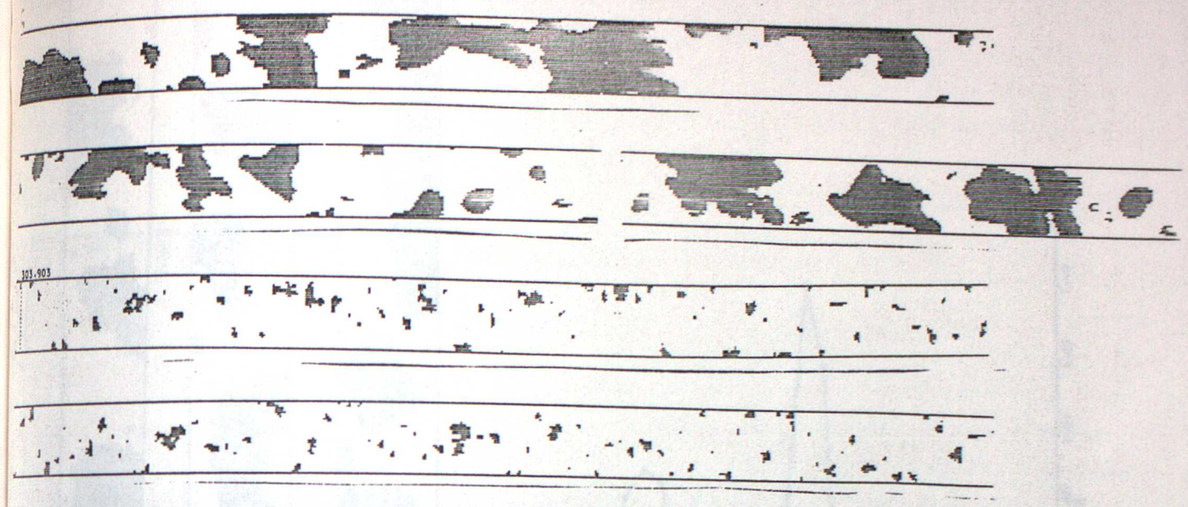


TEMPERATURE + 1.1°C ;

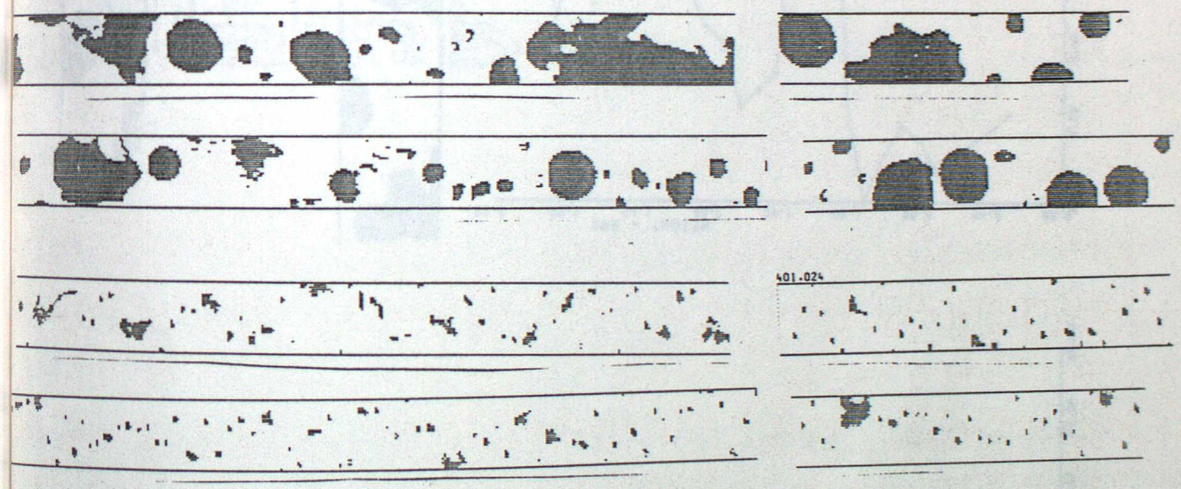


TEMPERATURE + 3.1°C ;

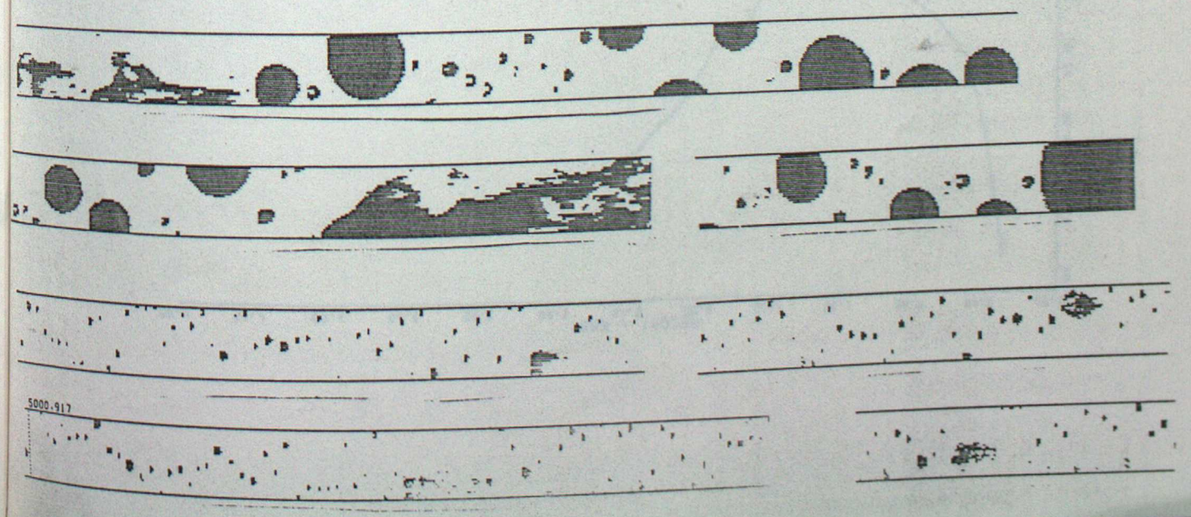

Figure 7

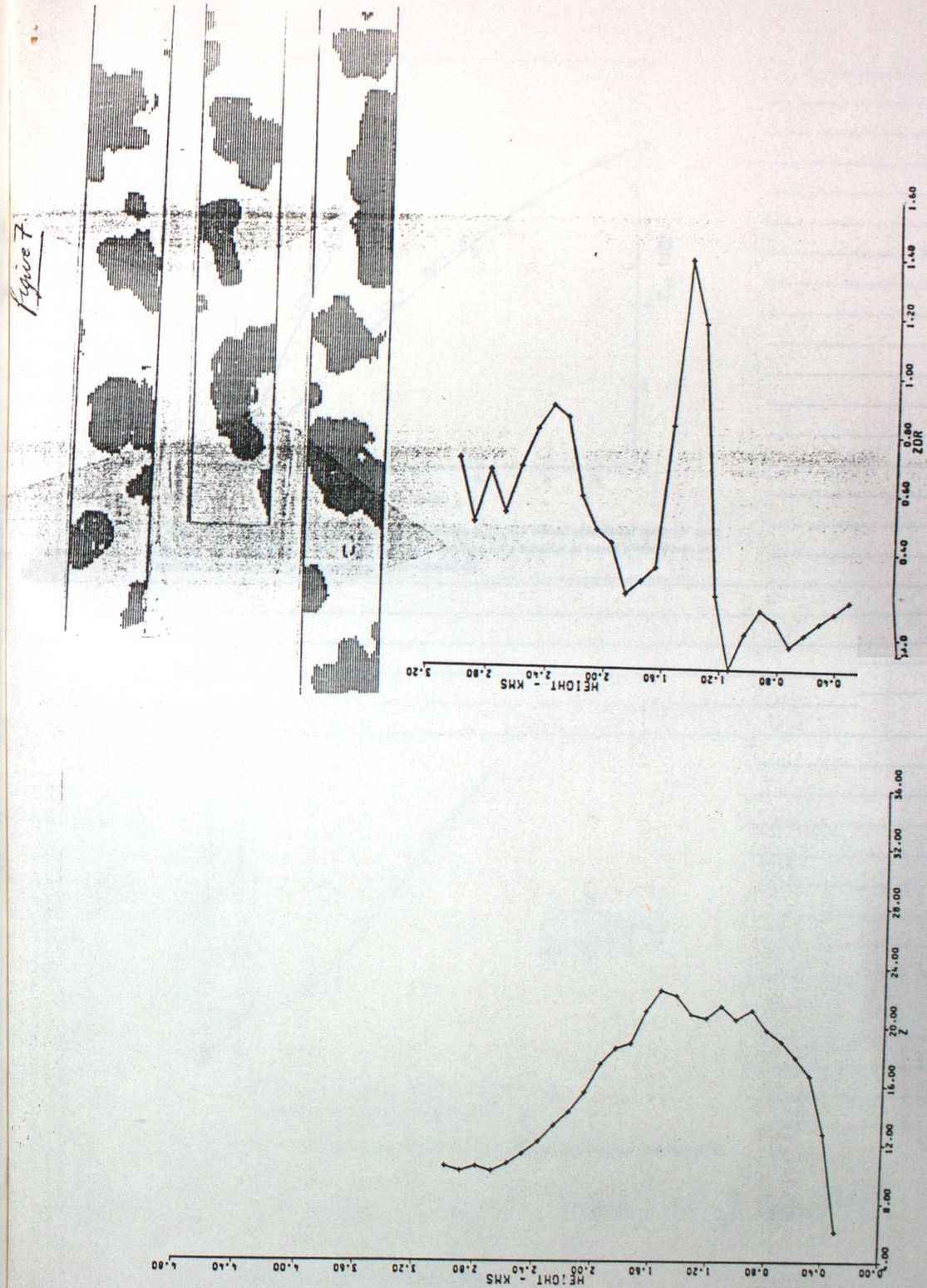
HEIGHT - KMS
0.40
0.80
1.20
1.60
2.00
2.40
2.80
3.20
ZDR
-0.40
0.00
0.40
0.80
1.00
1.20
1.40
1.60
HEIGHT - KMS
0.00
0.40
0.80
1.20
1.60
2.00
2.40
2.80
3.20
3.60
4.00
4.40
4.80
Z
0.00
8.00
16.00
20.00
24.00
28.00
32.00
36.00

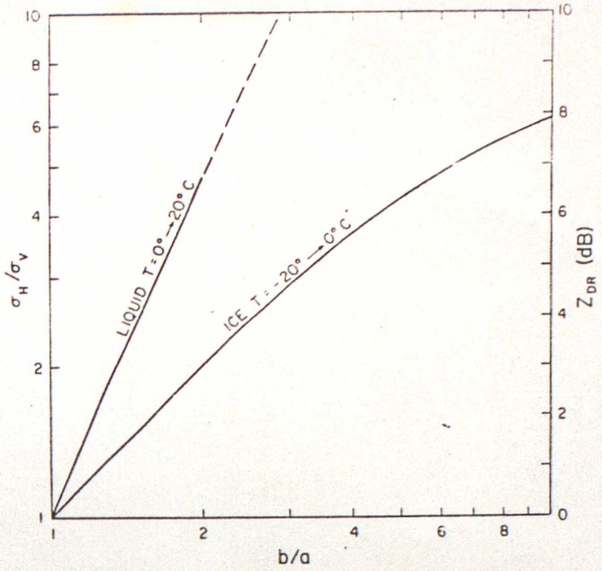


Fig. 8 . The ratio of backscatter cross sections $\sigma_H/\sigma_V$ for oblate spheriodal scatterer as a function of its axis ratio. The dashed portion of the line for a liquid is at ratios where drops are unstable; however, it can be used for water-coated ice.

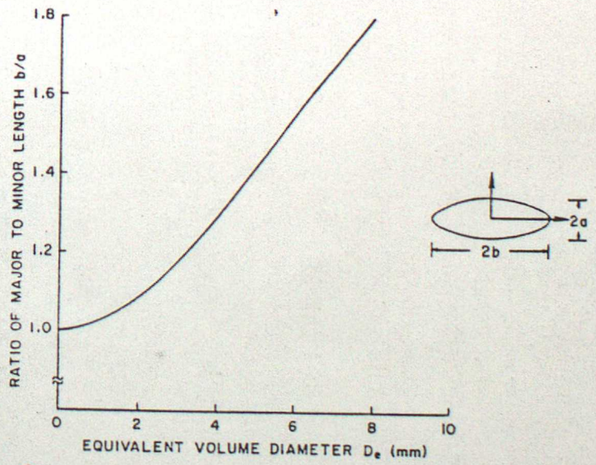


Fig. 9 . The ratio of the major axis length to minor axis length ($b/a$) as a function of $D_e$ given by Eq. (8.35)

(8.35) $D_e = 2\{(T_s/g\rho_w)[(b/a)^2 - 2(b/a)^{1/3} + 1](b/a)^{1/3}\}^{1/2}$

$T_s$ = Surface tension of water
$\rho_w$ = water density